BIOMATERIALS FOR THE CENTRAL NERVOUS SYSTEM

Contract No. NO1-NS-1-2338

Quarterly Progress Report #2

April 30, 2002

The University of Michigan and
The University of Utah

David C. Martin and Patrick A. Tresco

Quarterly Progress to:	National Institute of Health
Contract Monitor:	William Heetderks, Ph.D.
Research Contract	"Biomaterials for the Central Nervous System"
Contract No.	NO1-NS-1-2338
Principal Investigators:	David C. Martin and Patrick A. Tresco
Date:	April 30, 2002

Overview

This report is a summary of our activity in the second quarter of our contract, corresponding to the period from January 31, 2001 to April 30, 2002. We discuss our work to develop polymer films for the surface modification of neural prosthetic devices and the *in-vitro* and *in-vivo* testing of these modified electrodes.

In this quarterly report we first discuss results from the Martin group in the electrical characterization of PEDOT-functionalized electrodes. In particular, we discuss impedance spectroscopy results that have made it possible for us to extract information about the relationship between coating composition and structure and electronic properties. These results emphasize the utility of fuzzy coatings that have enhanced surface area for promoting efficient signal transport. We have also been able to obtain mechanical properties information from the coatings by nanoindentation, and these results are reported. Finally, we also relate information about the development of hydrogel coatings with controlled gradients in composition. We have confirmed the ability to encapsulate biological factors into biodegradable polymer microspheres that can then be incorporated into the coatings to provide controlled release of active substances.

We then discuss the results from the Tresco group on the biological characterization of neural probes. This includes information about the tissue response as a function of time for the non-coated controls. In this past quarter the Martin group prepared a series of electrochemically depostited polypyrrole-peptide and electrospun protein polymer coated probes, and these have now been sent to Utah and are under active investigation. Our future plans are to use the information learned by the Utah group about the *in-vitro* and *in-vivo* response of polymer-coated probes to develop improved materials systems.

PEDOT/PSS coatings

In the last quarterly report we described the electrochemical deposition of conducting poly(3,4-ethylenedioxythiophene) (PEDOT) using poly(styrene sulfonate) (PSS) counterion. Here, we discuss the electrical characterization and modeling of PEDOT/PSS films using impedance spectroscopy. We have reported previously the impedance spectroscopy performed on both uncoated and coated electrodes to examine the electrical properties of the coatings (Figure 1). It was found that impedance magnitude of the polymer coated electrodes were significantly lower than the uncoated gold electrodes. At 1 kHz, for all the films with various thicknesses, the impedance modulus dropped 2 orders of magnitude and the phase angle dropped from 80 degrees for gold to 10 ~ 15 degrees. Lowering the impedance without changing the geometric area of the electrode presumably will help to increase the detection sensitivity to neural activity.

In this quarter of research, an equivalent circuit approach was used to analyze the EIS data. Often, an equivalent circuit model which fits the EIS data will suggest some chemical model, process, or mechanism which can be proposed and tested. Some electrochemical and physical characteristics of the system can be discovered qualitatively and quantitatively. By observing the Nyquist plot of the impedance spectroscopy of the PEDOT coated electrode (Figure 1b), one can notice two distinct regions: a Warburgh diffusion impedance with a characteristic 45 degree slope at the high frequency region and a relatively pure capacitive region at low frequency region. A circuit model consisting of a solution resistance R_S in series with a finite-length Warburgh diffusion impedance component Z_D was built using electrochemical analysis software ZsimpWin V 2.0. The finite-length Warburgh diffusion impedance Z_D is defined as

$$Z_D = \frac{(\tau_D / C_D)\coth(j\,\omega\tau_D)^{1/2}}{(j\,\omega\tau_D)^{1/2}}$$

where τ_D is a diffusional time constant, C_D is a diffusional pseudocapacitance and τ_D/C_D can be defined as a diffusional resistance R_D [Macdonald 1987]. The trajectory of the simulated plot is consistent with the experimental plot but the individual data points deviate from the experimental data in many regions (% error of |Z| is within the range of ± 5%). A similar model for PEDOT/PSS film electrochemically deposited on Pt disk electrode was suggested in [Bobacka 2000]. In this model, a capacitance C_d was added in series (Figure 2). The addition of the capacitor improved the quality of the fit significantly. We built the same model (RTC model, where T represents the finite-length Warburgh Diffusional Impedance in the ZSimpWin software) and found a much better agreement between the simulated and the experimental data (Figure 3). The % error of |Z| is within the range of ± 1%. Parameters such as R_S, τ_D, C_d, C_D and R_D can be obtained from the circuit model equation. The RTC model was applied to Impedance Spectroscopy of PEDOT/PSS films deposited with a deposition charge of 5, 10 and 20 μC. The fitting is acceptable in all 3 cases with a χ^2 value below 1.5×10^{-3}. In all cases, the solution resistance is the same (9.5±0.3 kΩ). This is a strong support of the RTC model, since all the experiments were done using the same electrolyte solution and same electrochemical cell. The diffusional resistance R_D, on the other hand, increases as the film gets thicker (Figure 4). This is a good indication that R_D is a property of the bulk polymer film. Notice that the R_D vs. deposition charge shows a linear relationship between 5 ~ 20 μC, but the slope changes as the plot

approaches 0 μC. This discontinuous change of slope indicates a discontinuous change in the physical and electrochemical properties of the system such as film structure and morphology, and interfacial charge transport mechanisms. Many investigators have reported that conducting polymers grow on electrodes in a two-step process [Wang 1993; Silk 1998]. The initial growth results in a very dense and smooth film. When it reaches a certain thickness, the polymer film starts to become porous and fuzzy with lots of water content incorporated. The very thin dense film provides a pure capacitive signal transport barrier which is fundamentally different from the thick porous film.

In [Bobacka 2000] the physical meaning of the C_d was not clear but was tentatively assigned as the electronic part of the bulk capacitance, while C_D was considered the ionic part of the bulk capacitance. We calculated C_{total} when C_d and C_D are in series, and plotted these three capacitances vs. deposition charge (Figure 5). All three capacitance values increase linearly with the film thickness. Notice that the C_{total} is more dominated by the diffusional pseudocapacitance C_D, which is different from the result in [Bobacka 2000].

The diffusion time constant vs. deposition charge was plotted in Figure 6. It appears that τ_D increases linearly with increasing deposition charge. According to $D = L^2/\tau_D$, and assuming that the thickness of film is the diffusion length L, we can obtain the apparent diffusion coefficient D. The estimated thickness of film deposited with 5 μC is 1 μm from the side view of optical image. The calculated diffusion coefficients are 1, 2.4, and 4.7×10^{-6} cm^2/s respectively for film thickness of 1, 2, 4 μm. In [Bobacka 2000], the apparent D was reported to vary from 10^{-8} to 10^{-7} cm^2/s for the thickness range of 0.1 to 1.5 μm. This increase of apparent D with increasing thickness of film was correlated to the microstructure of the film. PEDOT film starts with a dense smooth layer. Very rapidly, it becomes porous and fuzzy as shown in Figure 7. One can imagine that a large amount of electrolyte solution can access the internal structure of the film through those pores. [Ghosh 1999] reported that PEDOT/PSS forms a highly swollen hydrogel with high surface area. Such an open film structure will allow for fast transport of ions in the supporting electrolyte phase and as a result, the effective diffusion length of the ions in the polymer phase is much smaller than the actual total thickness of the film. It is reasonable that the calculated D (10^{-8} cm^2/s) of the thinnest film (0.1 μm) in [Bobacka 2000] is the closest to the actual diffusion coefficient D. Assuming that this value is also characteristic of ionic transport kinetics through the polymer in our system, we estimate that the actual diffusion length of our 1 μm film would be 0.1 μm, which is 10 times smaller. A schematic of the open film structure of PEDOT deposited on a gold electrode is shown in Figure 8. It shows that electrolyte solution can get access into the inner pores of the film which shortens the actual diffusion length of ions with the bulk of the polymer film. Our results on impedance analysis clearly demonstrate that the effective transport properties of the polymer can be significantly improved with a tailored, fuzzy and porous morphology.

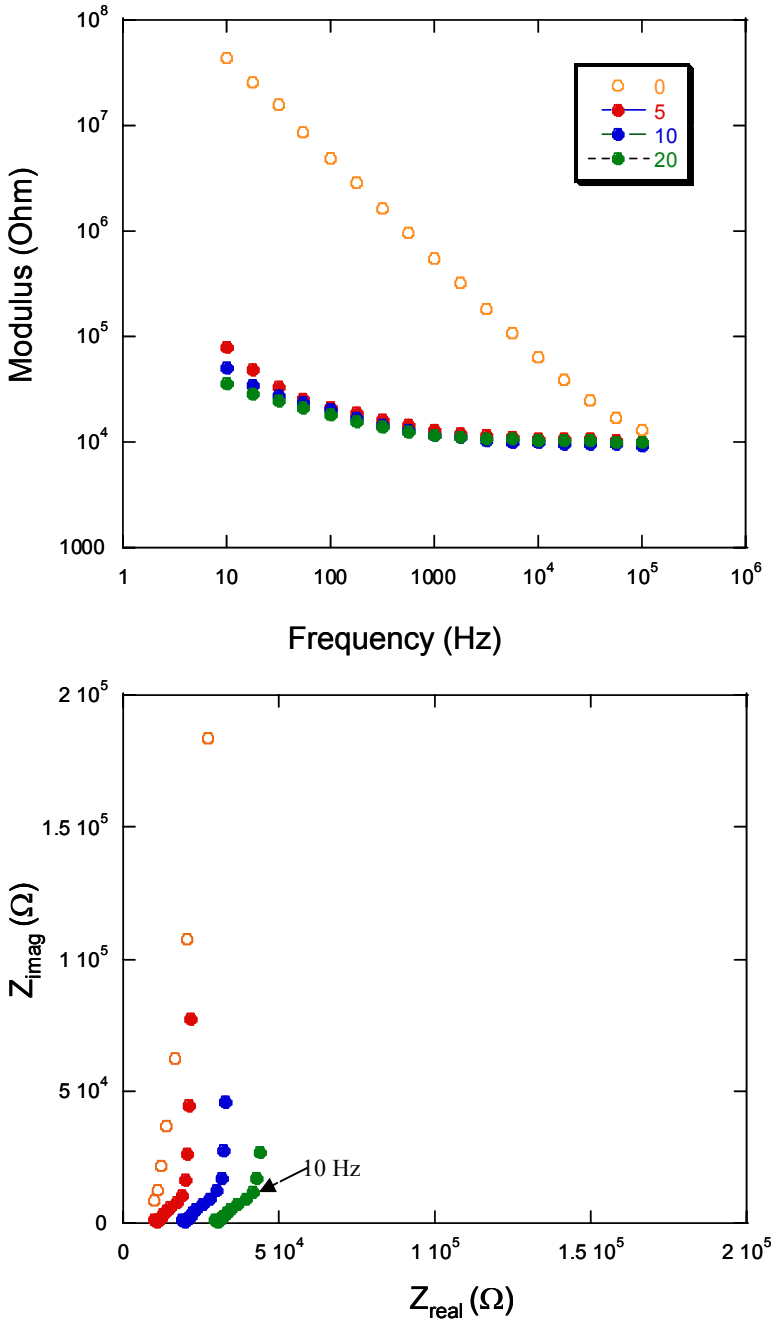

Figure 1. Impedance spectroscopy of PEDOT / PSS deposited on the gold electrode (with different deposition charge of 5, 10 and 20 μC) in comparison with the bare gold electrode. Top: Bode plot of Modulus vs. Frequency, Bottom, Nyquist plot of Z_{imag} vs. Z_{real}. Frequency range is from 10 to 100 kHz.

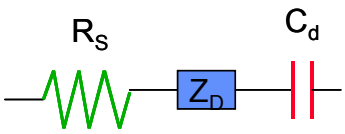

Figure 2. Equivalent Circuit Model for PEDOT/PSS on gold microelectrode. R_s is the solution resistance, Z_D is the finite-length Warburgh diffusion impedance element and C_d is bulk (electronic) capacitance.

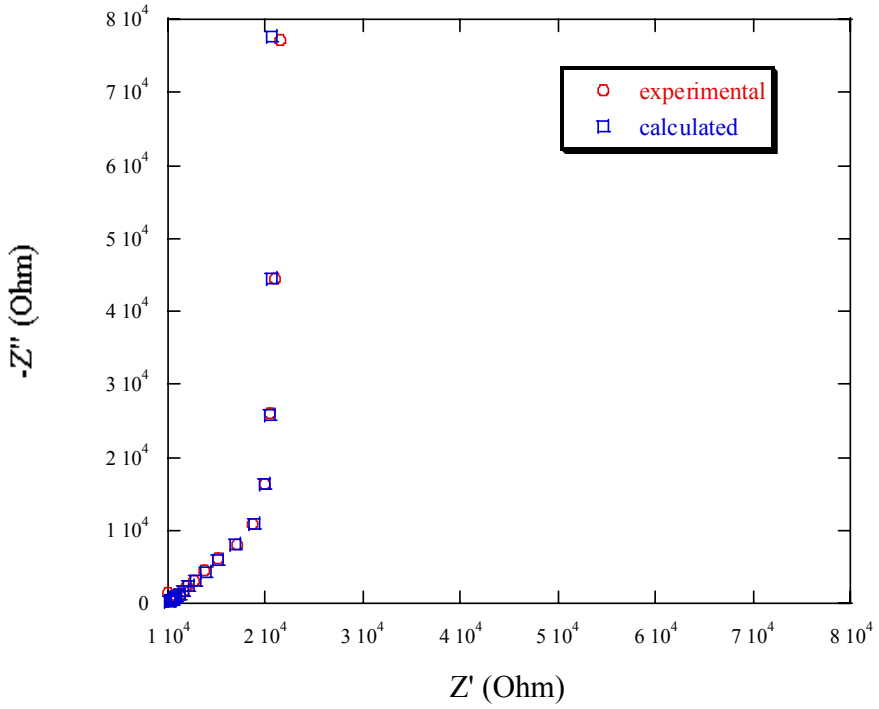

Figure 3. Impedance Spectroscopy of PEDOT/PSS on gold microelectrode. The polymer was deposited using deposition charge of 5 μC. Red sphere is the experimental data and green square is the simulated data using the equivalent circuit model shown in Figure 6 ($\chi^2 = 1.1 \times 10^{-3}$). R_S = 9.8 kΩ, τ_D = 0.0094 sec, C_d = 0.67 μF, C_D= 0.30 μF.

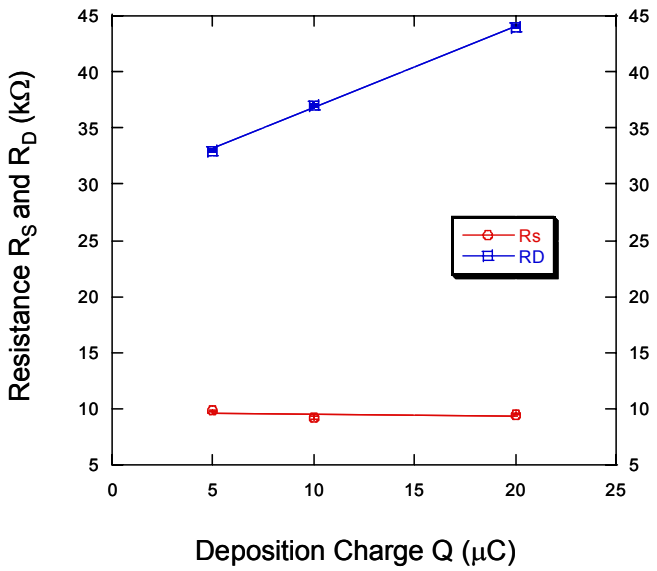

Figure 4. Resistance R_S and R_D as a function of deposition charge for film PEDOT/PSS in 0.1 M PBS solution.

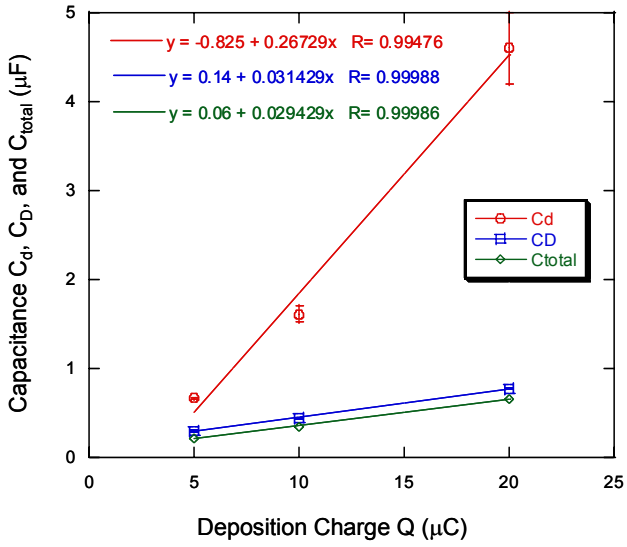

Figure 5. Capacitance C_d , C_D and C_{total} as a function of deposition charge for PEDOT/PSS film in 0.1 M PBS solution.

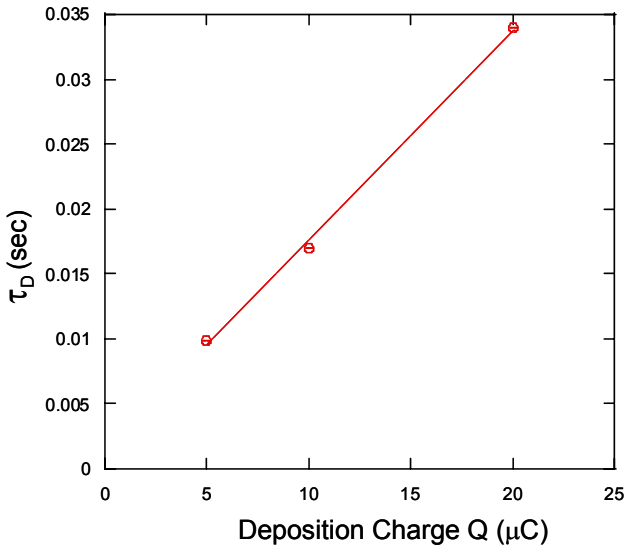

Figure 6. Diffusion time constant τ_D as a function of deposition charge for PEDOT/PSS film in 0.1 M PBS solution.

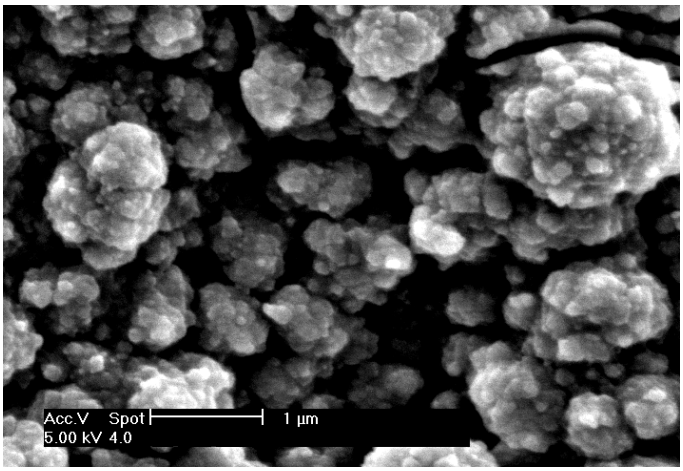

Figure 7. Scanning Electron Micrograph of PEDOT/PSS film deposited on gold microelectrode.

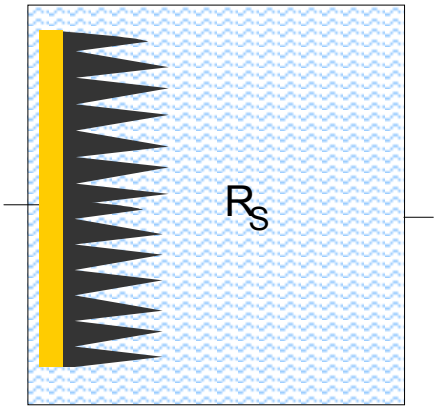

Figure 8. Schematic of an open structure of PEDOT film deposited on a gold electrode. Electrolyte can get into the pores of the film so that the diffusion length of electrolyte in the bulk of PEDOT is much smaller than the film thickness.

Nanoindentation of PPy/peptide coatings

A goal of our research is to create films with controlled gradients in mechanical properties to mediate the large differences in properties between hard, microfabricated neural implants and the soft tissue of the CNS. Our group has previously used nanoindentation methods to obtain information about the deformation behavior of biocompatible polymer thin films. The instrument can continuously measure force and displacement as an indentation is made. The indentation load-displacement data thus derived can be used to determine the mechanical properties even when the indentations are too small to be imaged conveniently. The indenter used in this study was a Nanoindenter II. Nanoindentation was performed with a conical diamond indenter with a spherical tip of which the radius was 1μm. Loads ranged from 0-4mN. Loading and unloading rates were 0.4mN/s.

In order to ensure that the indenter will not touch the substrate, the coating must be thick enough for the indentation. The thickness of the conducting polymer films on the electrode sites could be estimated from the optical images using NIH image software. According to previous data, the thickness of the coating obtained under the deposition condition was estimated to be 5μm (according to the current density and time adopted). Five individual points were selected to be indented. From Fig. 9 we can see that the shapes were almost the same, indicating from another aspect that the coating was very homogeneous.

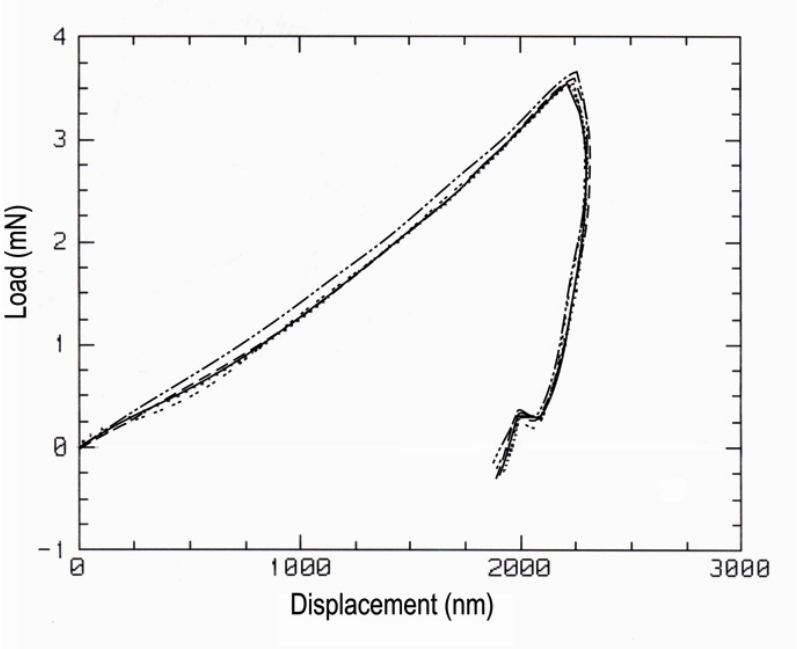

Figure 9: Nanoindentation of a 5µm electrochemically polymerized polypyrrole/bioactive peptide film.

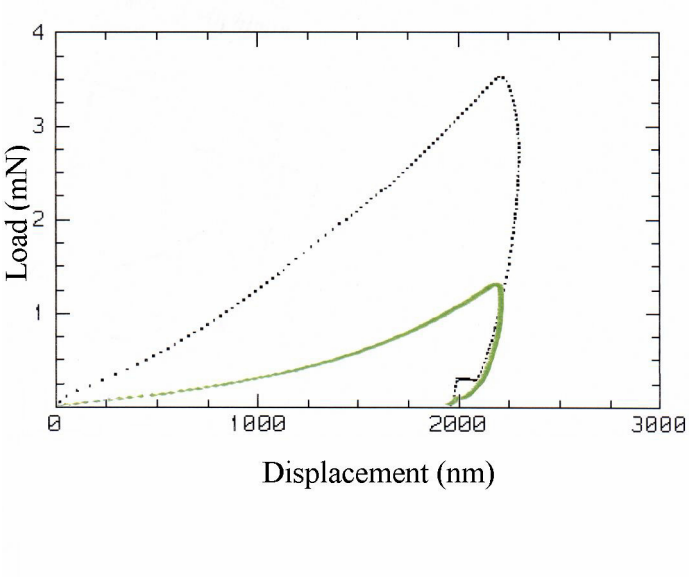

Figure 10: Comparison between the nanoindentation response of polypyrrole/peptide film (dashed) with electrospun protein polymer (green). Both films are highly compliant, and show that large strains can be accomodated without inducing failure.

By comparing the load-displacement curve with our previous results (Fig. 10) it is seen the conducting polymer coating exhibited the similar deformation behavior to that previously seen in the nanospun fibrous filaments of SLPF protein polymer. The slope of the curve increases with displacement, indicating that there is increase in effective modulus as a function

of displacement. We expect this response is primarily due to the plastic deformation and densification of the polymer film. It is known that the morphology of PPy/ CDPGYGIGSR coating is porous, and with the load the pores yield, plastically deform, and collapse, leading the density of the indented area to rise. This phenomenon can also be seen from SEM images (Figure 11). The deformation zone where the indentor contacted the sample shows a ragged edge between the region that has undergone plastic deformation and the usual nodular morphology of electrochemically deposited PPy/CDPGYGISR. Material densification in the center of the indentation can also be observed in the SEM.

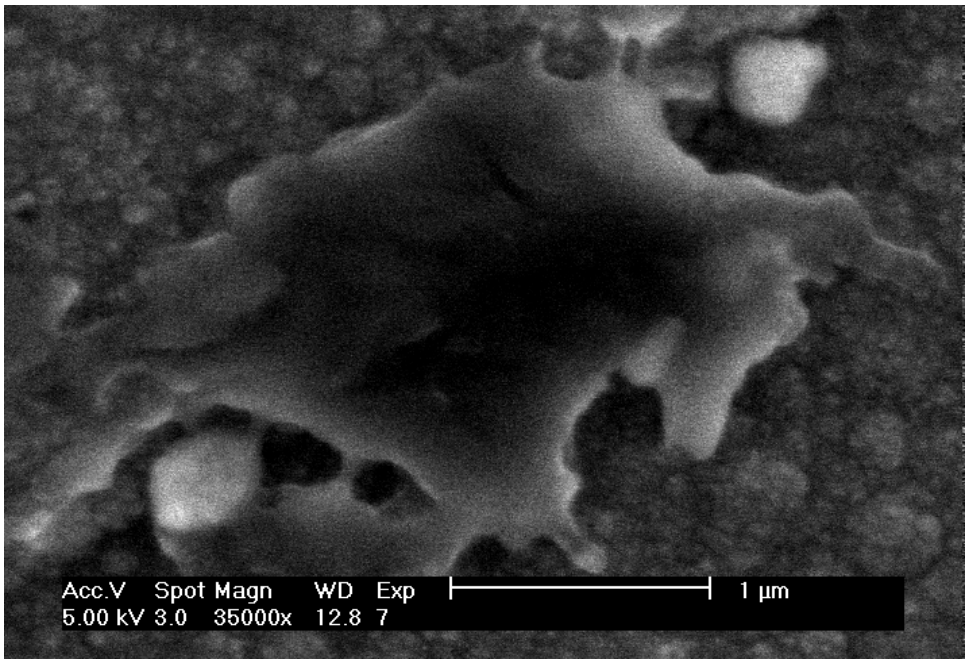

Figure 11: SEM image of the plastic deformation due to indentation on the surface of a polypyrrole/peptide coatings.

Using the load-displacement behavior of coatings, it was possible to calculate an apparent reduced modulus for the polymer thin films. Fig. 12 shows a graph of E* calculated from the indented sample. The effective modulus is about 1.3 GPa, and increases slightly with load. This value is reasonable for a relatively unoriented polymer solid. The stiffness is intermediate to that of silicon crystals (E ~ 150 GPa) and the soft tissue of the CNS (~100 kPa).

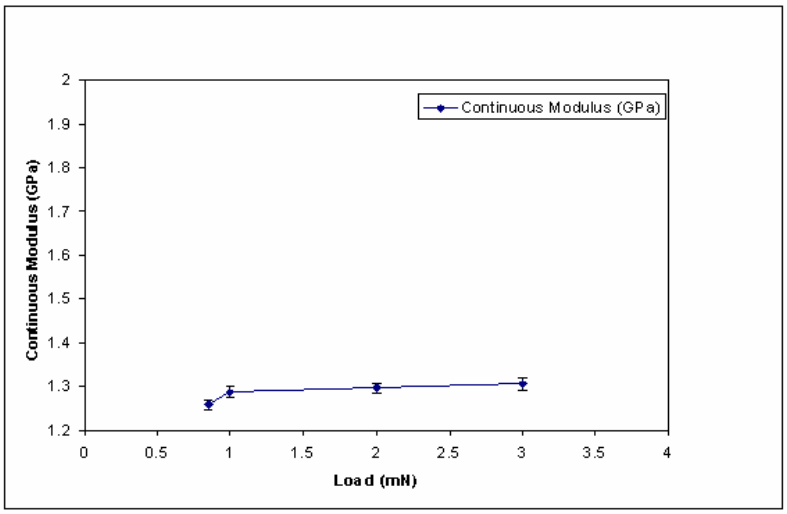

Figure 12: Apparent modulus of the polymer coatings (GPa) as a function of applied load (mN).

Hydrogel Chemical Gradient Coatings

Recently, we have devoted our efforts to making several layers of hydrogel coatings with controlled concentration gradients of Nerve Growth Factor. The pictures below show that the various layers of polymer can be formed on the probe. In these experiments the hydrogel was labeled with a ~1 M gm/mole blue dextran dye. The images show the formation of a graded coating with a blue inner layer, and a clear outer layer. The dark band in the middle of the image is the shank of the probe. The outer layer was itself composed from several dipping and drying steps, and stratification can be seen within this layer.

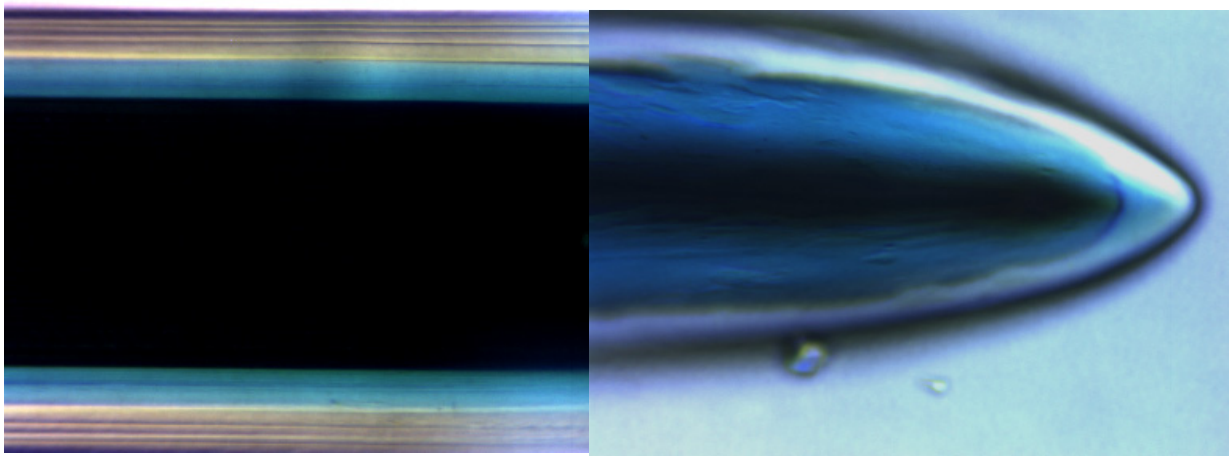

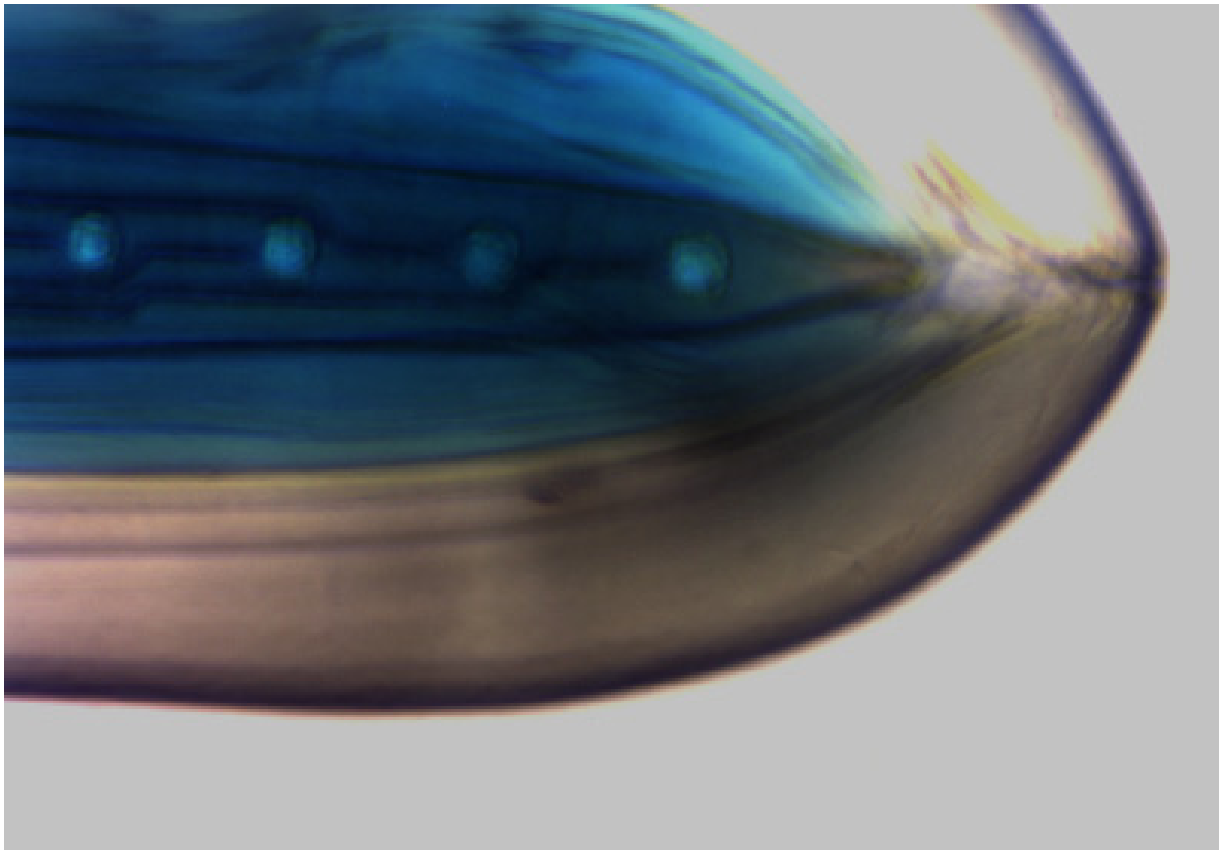

The tip of the neural probe can also be seen encapsulated within an inner blue layer and an outer clear layer. As discussed in last quarter's report, our intention is to insert the hydrogels into the tissue while dry and then allow them to reswell using the naturally available water in the environment.

Our immediate goal is to create gradients of growth factors that will attract neurons to the probe. However, the diffusivity of NGF in the hydrogel is likely too high, leading to rapid release of the biological factors. Therefore, PLGA micro-spheres may be attractive candidates to making stable gradients of NGF. PLGA is a well-known biodegradable polymer that is already in use in drug delivery systems. We are going to put the micro-spheres with different gradients of growth factor into the layers of hydrogel. These microspheres enclosed the biological active factors, and the rate of release can be changed by manipulating the thickness of the polymer shell and the composition of the polymer. PLGA microspheres can be made by following protocol that have been developed in Prof. David Mooney's laboratory:

1. Siliconize 9-5ml test tubes with Sigmacote and let dry overnight and rinse tubes with 1% BSA solution and let air dry to prevent growth factor absorption.
2. Prepare 1800 ml of 0.3% Poly vinyl alcohol and 7% ethyl acetate solution
3. Prepare 20 ml 5% solution of PLGA polymer in ethyl acetate.(emulsion solution 1)
4. Prepare 10 ml 1% PVA 7% ethyl acetate (emulsion solution 2)
5. Prepare solution of growth factor to appropriate concentrations for use at 100ul
6. Add 100 ul of growth factor solution to emulsion 1
7. Add 1ml of emulsion 2 to the 6 solution
8. Stir for 3 hours to allow the solvent to evaporate.
9. Filtrate it and lyophilize.

We have already confirmed that this procedure works well, and are using this protocol to place the microspheres within the hydrogel coatings on the surfaces of the neural probes.

REFERENCES

Bobacka, J., Lewenstam, A. and Ivaska, A. (2000). "Electrochemical impedance spectroscopy of oxidized poly(3,4- ethylenedioxythiophene) film electrodes in aqueous solutions." J. Electroanal. Chem. **489**(1-2): 17-27.

Ghosh, S. and Inganas, O. (1999). "Conducting polymer hydrogels as 3D electrodes: Applications for supercapacitors." Adv. Mater. **11**(14): 1214-1218.

Macdonald, J. (1987). Impedance Spectroscopy. New York, Wiley.

Silk, T., Hong, Q., Tamm, J. and Compton, R. G. (1998). "AFM studies of polypyrrole film surface morphology - II. Roughness characterization by the fractal dimension analysis." Synth. Met. **93**(1): 65-71.

Wang, Y. B., Yuan, R. K., Yuan, H. and Chen, Z. H. (1993). "Theoretical and Experimental Studies of Conducting Polymer Polyaniline Electrolyte Interface by Impedance Spectroscopy." Synth. Met. **55**(2-3): 1501-1508.

Quarterly Progress Report for the period February – April, 2002

From the Tresco Group, University of Utah subcontract for N01-NS-1-2338

OVERVIEW

In the current report we discuss our progress toward characterizing the cellular responses to uncoated and untreated microelectrodes. The findings will serve as control data and a source of comparison for specific surface coatings on microelectrode shafts and recording sites. We describe observations on the attachment of primary neural cells to probes in vitro as well as the host response to implanted untethered microelectrodes in adult rat brain.

CELL ATTACHMENT TO UNCOATED MICROELECTRODES IN VITRO

Introduction

In order to understand the biological activity of specific coatings for improving neural cell attachment, it is necessary to establish baseline cell behavioral characteristics on the unmodified electrode surfaces. We have examined the attachment of primary postnatal day 1 (P1) cortical astrocytes, adult meningeal fibroblasts, P1 hippocampal neurons, and P7 cerebellar granule neurons. Attachment under static culture conditions was quantified using immunofluorescent micrographs of the microelectrode surfaces after 24 hours of culture. In order to better approximate the soluble conditions that would ordinarily dominate in vivo, the microelectrodes were pre-incubated in medium containing 10% serum prior to the addition of the cells. All cells were plated at densities that approximate that which they would normally encounter following implantation into adult rat cortical parenchyma, that is, the normal cell number to surface area ratio (as determined during the last quarter and appearing in the 1st progress report, January 2002).

Materials and Methods

Preparation of Microelectrodes for Tissue Culture: performed as previously described in 1st quarterly report January 2002.

Isolation and culture of astrocytes: performed as previously described in 1st quarterly report January 2002. Astrocytes were first established in culture flasks and purified prior to plating onto the microelectrode surfaces.

Isolation and culture of adult meningeal fibroblasts: Adult female Sprague-Dawley rats were deeply anesthetized with a mixture of ketamine (70mg/kg) and xylazine (30mg/kg) injected i.p. Animals were perfused transcardially with 250mL of ice-cold 0.1M phosphate-buffered saline, decapitated, and their brains removed. Meninges were peeled away from the cortical surface, then processed as described for P1 meningeal fibroblasts in the first quarter progress report (January 30, 2002). Adult meningeal fibroblasts, like astrocytes, were first established in culture flask prior to being passaged onto the microelectrode substrates.

Isolation and culture of P1 hippocampal neurons: The hippocampus from P1 rat brains was dissected away from the surrounding brain and meningeal tissue was carefully peeled of the outer surface. The tissue was minced then placed into cation-free Hank's Balanced Salt Solution (HBSS) containing 1% (w/v) trypsin (Worthington) for 15 minutes at 37°C. Enzymatic dissociation was terminated by the additon of soybean trypsin inhibitor (SBTI; Worthington) followed by centrifugation at 300g for 15 minutes. Cells were resuspended in DMEM containing 0.1% (w/v) DNase and triturated through Pasteur pipettes of decreasing bore diameter. The resultant cell suspension was centrifuged then resuspended in DMEM containing 10% fetal bovine serum (FBS; Hyclone) and plated onto a petri dish that was previously coated with a solution of poly-D-lysine (500 ug/mL; Sigma). Cells were incubated on the poly-lysine dish for 10 minutes to remove a majority of the contaminating non-neuronal cell populations. The supernatant was collected, counted on a hemacytometer, and plated onto the microelectrode substrates.

Isolation and culture of P7 cerebellar granule neurons: Cerebella from P7 rats were dissected away from the brain and meninges carefully peeled away. The remaining steps of the preparation were carried out exactly as described above for P1 hippocampal neurons as described above.

Cell plating and culture: Isolated cells were plated onto microlectrode substrates at the following densities: astrocytes: 283 cells/mm^2, meningeal fibroblasts: 283 cells/mm^2, hippocampal and cerebellar neurons 372 cells/mm^2. All microelectrode substrates were first incubated overnight at 37°C in DMEM with 10% FBS prior to cell plating. All cells were cultured in DMEM containing 10% FBS for 24 hours. At this point, cultures were fixed in fresh 4% paraformaldehyde for 12 minutes at room temperature.

Immunofluorescence: Fixed cells were permeabilized for 5 minutes in 0.1M PBS containing 0.5% (v/v) Triton-X-100. The following primary antisera were applied: polyclonal antiglial fibrillary acidic protein (GFAP; Dako) diluted 1/1000, monoclonal anti vimentin (Sigma) diluted 1/1000, monoclonal anti beta-III-tubulin (Sigma) diluted 1/500. Appropriate secondary antibodies conjugated to Alexa 488 or Alexa 594 (Molecular Probes) were diluted 1/200. All antibodies were diluted in 0.1M PBS containing 4% goat serum and 0.1% sodium azide and were applied for 1 hour. Cell nuclei were stained with DAPI (Molecular Probes). When completed, the coverslips with attached microelectrodes were covered in Fluoromount-G and sealed by

covering with another coverslip. The resulting sealed coverslip "sandwich" was then tacked to a glass slide using UV-cure adhesive.

Cell attachment analysis: The number of cells attached to each microelectrode was counted visually using an epifluorescence microscope with a 20X objective. Total cell number for each electrode was scored (n=10).

Results and Discussion

Overall cell attachment to uncoated electrodes was low in comparison with traditional culture substrates such as tissue culture plastic and glass. Meningeal fibroblasts exhibited the greatest amount of attachment and cell spreading. Astrocytes exhibited a marked tendency to align along the longitudinal topography created by microelectrode trace paths. For both astrocytes and meningeal fibroblasts, attachment to the backside of the probe was slightly higher than the recording site side. Neuronal attachment was sparse with only a rare occurrence of process outgrowth. Where attached, neurons tended to form aggregates, a characteristic response to poorly adhesive surfaces (Figure U2-1). No preference was observed for neuronal attachment to the recording sites over the electrode shaft. The overall poor attachment by primary CNS neurons is not surprising in light of previous studies. For example fibronectin, the primary adhesive ECM protein

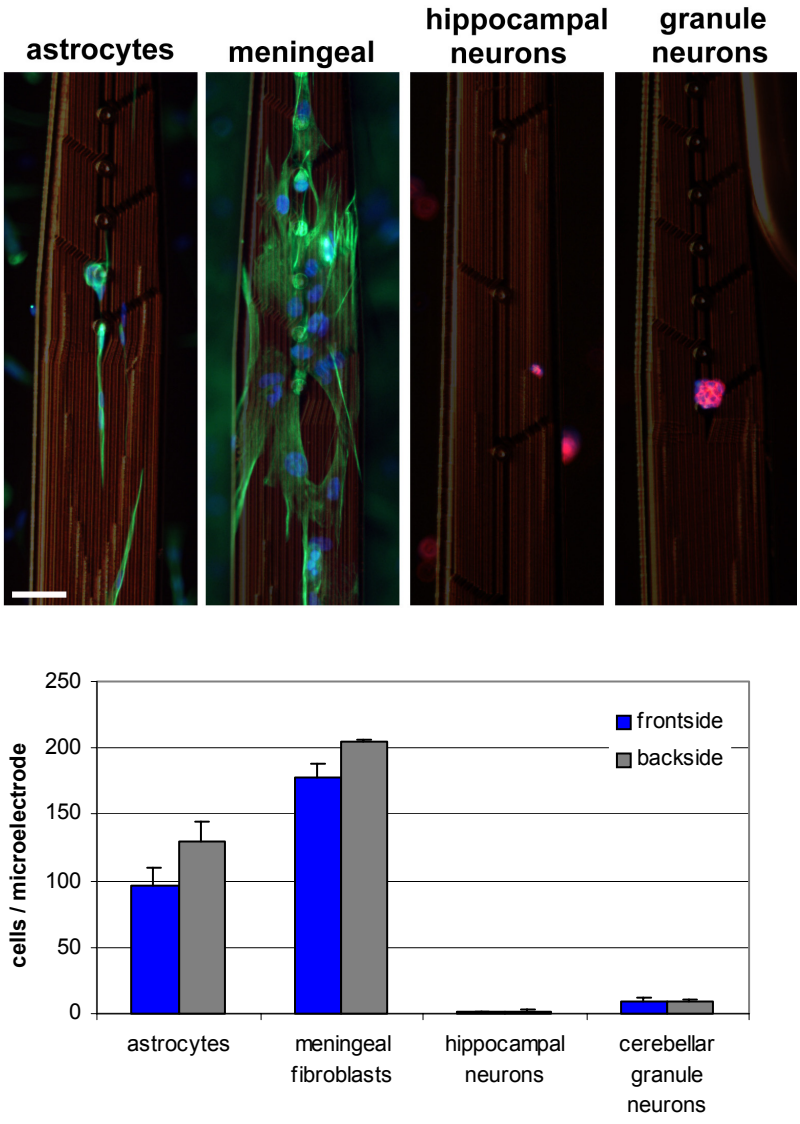

Figure U2-1. Cell attachment to uncoated microelectrodes in vitro. Representative photos are shown in the upper panel (scale bar = 50 microns). The number of attached cells in the static attachment assay is shown in the graph. Average values (+/- standard error of the mean, n=9) for attachment for both the front (recording-site side) and rear of the microelectrodes are shown.

in serum, is a poor substrate in vitro for many CNS neurons (Rogers et al, 1983). In contrast, astrocytes and meningeal fibroblasts are known to attach to a variety of surface chemistries in the presence of serum (Biran et al, 1999; Manwaring et al, 2001). Initial attachment of either astrocytes or meningeal fibroblasts eventually resulted in complete colonization of the substrate.

In summary, we found the microelectrode surfaces supported a far greater degree of astrocyte and meningeal attachment than neuronal attachment. It is important to note that the amount of attachment in this study differed from our previous report, where astrocytes and meningeal fibroblasts were attached over almost the entire electrode surface (1st Progress Report, January 2002). The principle difference between the two experiments was the initial cell plating density. In the current study, we plated cells at a cell number to surface area ratio that would most closely match the actual ratio at the interface of a microlectrode following implantation into the adult rat cortex as determined from stereological analysis. This seeding density is far lower than the densities used in the earlier study. These data indicate that uncoated microelectrodes, treated only with dilute serum, are a poor adhesive surface for central neurons.

HOST RESPONSE TO UNCOATED ELECTRODES IMPLANTED INTO ADULT RAT BRAIN

Introduction

In order to develop an understanding of the basic tissue response to microelectrode implants (that will later serve as the baseline controls for all subsequent implants) and to reduce to practice the handling and surgical implantation of the devices in the absence of any additional specific experimental coatings, we examined the host wound healing response to untethered and uncoated microelectrodes. Cohorts of animals were implanted and sacrificed after 1 week, 2 weeks, 4 weeks, and 12 weeks. At the time of this report, the 12 week time point is still ongoing, and thus only data from the first three time points is presented here. The response of microglia, macrophages, and astrocytes was assessed with cell-type-specfic antisera. We also report on the use of the lipophilic tracer DiI as a tool to fluorescently label the microelectrode tract, so that one can easily and unambiguously identify the path of microelectrode entry after the electrode is retrieved.

Materials and Methods

Preparing microelectrodes: Unthethered 5mm single shank acute microelectrodes with various site spacings were washed in distilled water, sterilized by immersion in 70% ethanol for 15 minutes, then washed in sterile distilled water.

Animal surgery and implantation: Adult male Fischer 344 rats (225g-250g) were anesthetized with a cocktail of ketamine (65mg/kg), xylazine (7.5mg/kg), and acepromazine (0.5mg/kg). Upon reaching full anesthesia, the animals' head is shaved with a surgical clipper and eyes

covered with ophthalmic ointment. The scalp is rendered aseptic by liberal application of isopropanol followed by butadiene. The animal is then transferred to stereotactic frame. A midline incision was made, then the skull was trephinated (3mm diameter) to expose the underlying brain. After carefully removing the dura, 2uL of DiI (2mg/mL in DMSO; Molecular Probes) was applied to the underlying pia. A single microelectrode was carefully lowered through the pool of DiI into the brain at coordinates +0.2mm bregma and 3mm lateral. Before implanting the microelectrode, the tab at the top of the probe where the bonding sites are located was broken-off so that the entire electrode shaft could be placed into the brain. The bone plug was replaced, and the scalp sutured with 5/0 silk sutures. After recovering under observation, the animals were returned to their cages. Cohorts of 9 animals were implanted for each time point. Six control animals (no surgery) were also included.

Euthanasia of animals, tissue preparation, probe retrieval: At various time points after implantation, cohorts of animals were deeply anesthetized with a mixture of ketamine (70mg/kg) and xylazine (30mg/kg). Animals were perfused transcardially with 250mL of ice-cold 0.1M PBS, followed by 250mL of fresh paraformaldehyde (4% w/v in 0.1M PBS). Animals were decapitated and their brains carefully removed from the skull. Brains were post-fixed overnight in 4% paraformaldheyde. Before sectioning the tissue, the electrodes (usually visible at the surface of the brain), were retrieved with sharp microdissection forceps and processed for immunostaining. The brains were then blocked and cut into 50 micron horizontal or coronal sections with a Vibratome.

Immunostaining sections and photos: Vibratome sections were permeabilized with 0.5% triton X-100 (Sigma) in PBS for 30 minutes and blocked using dilute goat (4%) serum in PBS containing 0.3% triton. In general, sections were incubated in primary antibody diluted in blocking solution overnight (18-20hrs) at 4°C. The following primary antibodies were used: polyclonal antisera against glial fibrillary acidic protein (GFAP; 1:1000; Dako Corp.); monoclonal antiserum against vimentin (1:1000; Sigma); monoclonal antiserum ED-1 (recognizes activated microglia and macrophages; 1:1000, Serotec), and the monoclonal antiserum OX-42 (recognizes resting microglia and macrophages; 1:1000; BD/Pharmingen). Blocking and primary antibody solutions did not contain triton for staining membrane antigens (ED-1 and OX-42). Sections were then rinsed in PBS followed by incubation in the appropriate secondary antibodies conjugated with Alexa 488 (Molecular Probes). In some cases, amplification was required and a biotinylated secondary antibody was followed by a streptavidin-conjugated Alexa 488 (Molecular Probes) applied for 50 minutes at room temperature to visualize the reaction. All secondary and tertiary reagents were used at a dilution of 1:220 from manufacturer's stock concentration. All sections were counterstained with DAPI to identify cell nuclei.

Stained sections were visualized using the appropriate fluorescent filters on a Nikon E600 epifluorescence microscope. Retrieved microelectrodes were similarly stained except they were not pre-blocked and primary antibody was applied for only 1 hour at room temperature. Representative images were captured using a CCD camera (CoolSnap, RS Photometrics). For double and triple-stained samples, each image was taken using only one emission filter at a time. Layered montages were then prepared using Adobe Photoshop software on a PC computer.

Results and Discussion

In order to investigate the CNS host response to microelectrodes, cohorts of adult male rats were implanted with untethered and uncoated microelectrodes (5mm acute probes) and sacrificed at 1 week, 2 weeks, and 4 weeks. The response of macrophages and microglia (assessed by ED-1 and OX-42 staining) as well as astrocytes was investigated by indirect immunofluorescence of 50 micron tissue sections.

In general, the implants appeared to be tightly in place within the surrounding brain tissue. The top of the implant shaft was visible at the brain surface, often covered with a thin sheath of fibrous tissue (Figure U2-2). The implant tract that remained after retrieval of the microelectrode often retained a shape that matched the proportions of the microelectrode. In fact, at the 4 week time point, the surrounding tissue had conformed to the implant surfaces to such a degree that the longitudinal pattern of the traces were observed on the adjacent tissue (data not shown). There was none or very little accumulation of hemosiderin or red blood cells at the implant site at all time points indicating minimal vascular damage.

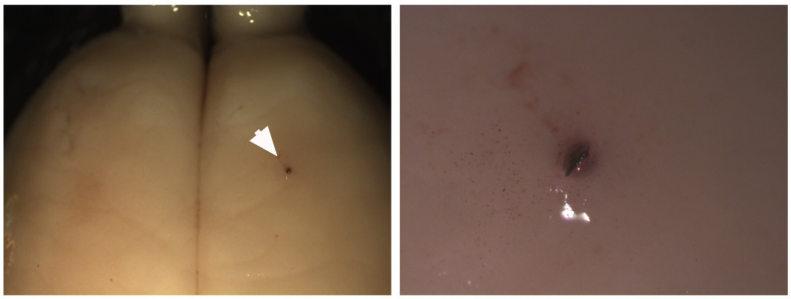

Figure U2-2. Representative photos of microelectrodes visible from the unstained brain surface prior to retrieval and immunostaining (left panel) low power, and (right panel) higher panel.

Due to the small size of the microelectrodes, it is often difficult to determine the implantation tract (unpublished communication form members of the CNCT, University of Michigan) once the microelectrode is retrieved from fixed brain tissue, especiallyin cases when the host response is subtle. To circumvent this potential problem, we developed a method of post implantation tract imaging that utilized the lipophilic dye DiI to label the implant tract during the initial implant procedure. The method consists of adding two microliters of dye t the surface of the brain immediately under the implantation site. The dye consistently and reliably labeled the entire implant tract, and remained detectable at all time points examined (Figure U2-3). The dye may also be of benefit as a retrograde tracer to specifically identify neurons with projections adjacent to the implant site to address the issue of specific neuronal interaction at modified recording sites. We intend to pursue this possibility in future experiments.

Analysis of the host response revealed a marked accumulation of microglia and macrophages at the implant interface (Figures U2-4 and U2-5). ED-1 and OX-42 staining after 1 week intensely labeled a dense layer of cells that were either macrophages or microglia. We observed that ED-1 staining diminished at 2 and 4 weeks. ED-1 immunoreactivity in microglia is indicative of an activated state and labels microglia with ameboid morphology, which is also a characterstic feature of microglial activation. Despite the temporal decrease of ED-1 around the implants, a band of OX-42 immunoreactive cells with ameboid morphology remained at the implant interface at all time points. The persistence of macrophages/microglia accompanied with a

decrease in ED-1 staining suggests a possible decrease in activation state over time; however, because of the persistence of ameboid OX-42 immunoreactive cells it is difficult to conclude the macrphage/microglia reactivity was declining. Nevertheless, it appeared that at the time points examined, the microelectrode host interface primarily involved microglia and/or macrophages.

The astrocyte response to the implanted microelectrodes was typical for an indwelling implant. The pattern and intensity of GFAP expression around the implanted microelectrode at all time points was greater than that of control uninjured tissue. At 1 week, GFAP immuno-reactivity markedly increased adjacent to and around the implant site, accompanied by the appearance of numerous hypertrophied astrocytes (Figures U2-4 and U2-5). By 2 weeks, the zone of intensely GFAP$^+$ cells contracted into a smaller area around the implant site. By 4 weeks, gliosis was still evident, however, both the intensity and GFAP immunostaining and the number of hypertrophied astrocytes appeared to decline in comparison to the early time points. Close examination of the tissue directly adjacent to the gap left by the retrieved microelectrodes revealed that GFAP immunoreactive cells were often 1 to 2 cell layers removed from the implant interface. The cells directly adjacent to the implant were identified as microglia or macrophages by ED-1 and OX-42 immunostaining. Indeed, as will be discussed later, the only cells that remained on the retrieved probes were OX-42 positive.

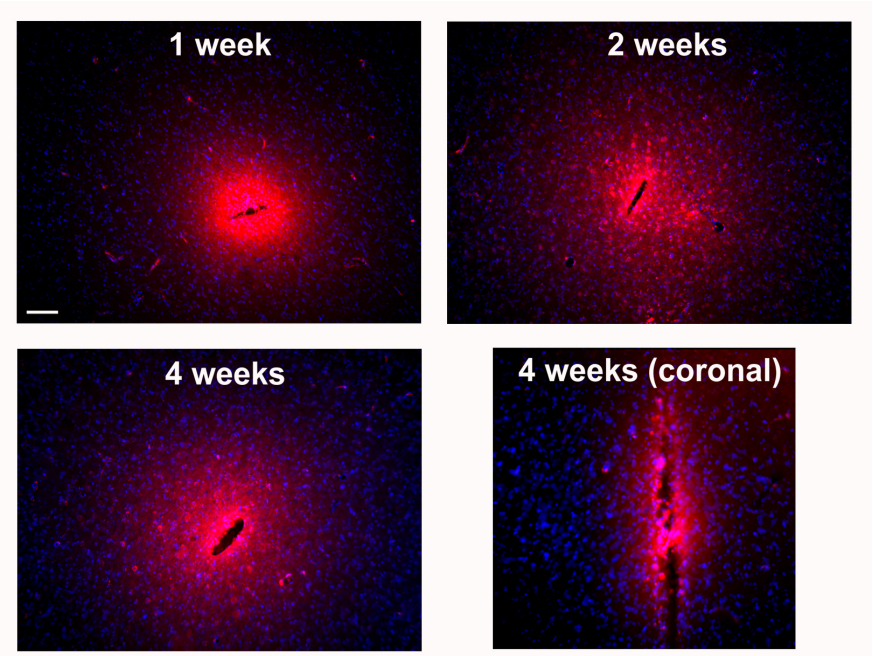

Figure U2-3. The microelectrode implant tract remains labeled with DiI over time. The dye (red) is visible in both horizontal and coronal sections of the implant. Nuclei are counterstained in blue with DAPI All of the sections are at the level of the cerebral cortex. Scale bar = 100 microns.

Like GFAP, the intermediate filament vimentin is also known to be upregulated by astrocytes (cells that are both GFAP$^+$ and vimentin$^+$) in response to CNS injury. However, vimentin is not cell-type-specific, and can also label fibroblasts and a variety of CNS precursor and stem cell populations. Unlike GFAP, detectable vimentin expression in the intact adult brain is limited to only a few locations. We observed marked vimentin upregulation adjacent to the implant site at all time points (Figures U2-4 and U2-5). Many vimentin$^+$ cells were likely also GFAP$^+$, as their morphologies were identical to GFAP+ cells in tissue sections from the same time points.

Unlike the pattern of GFAP immunoreactivity, vimentin expression did not appear to diminish over time.

In summary, the host response to microelectrodes diminished in degree as implant time increased. However, by the latest time point we examined (4 weeks), there remained elements of both an inflammatory response (microglia/macrophages) as well as gliosis, and direct contact with the electrode surface appeared to be dominated by microglia.

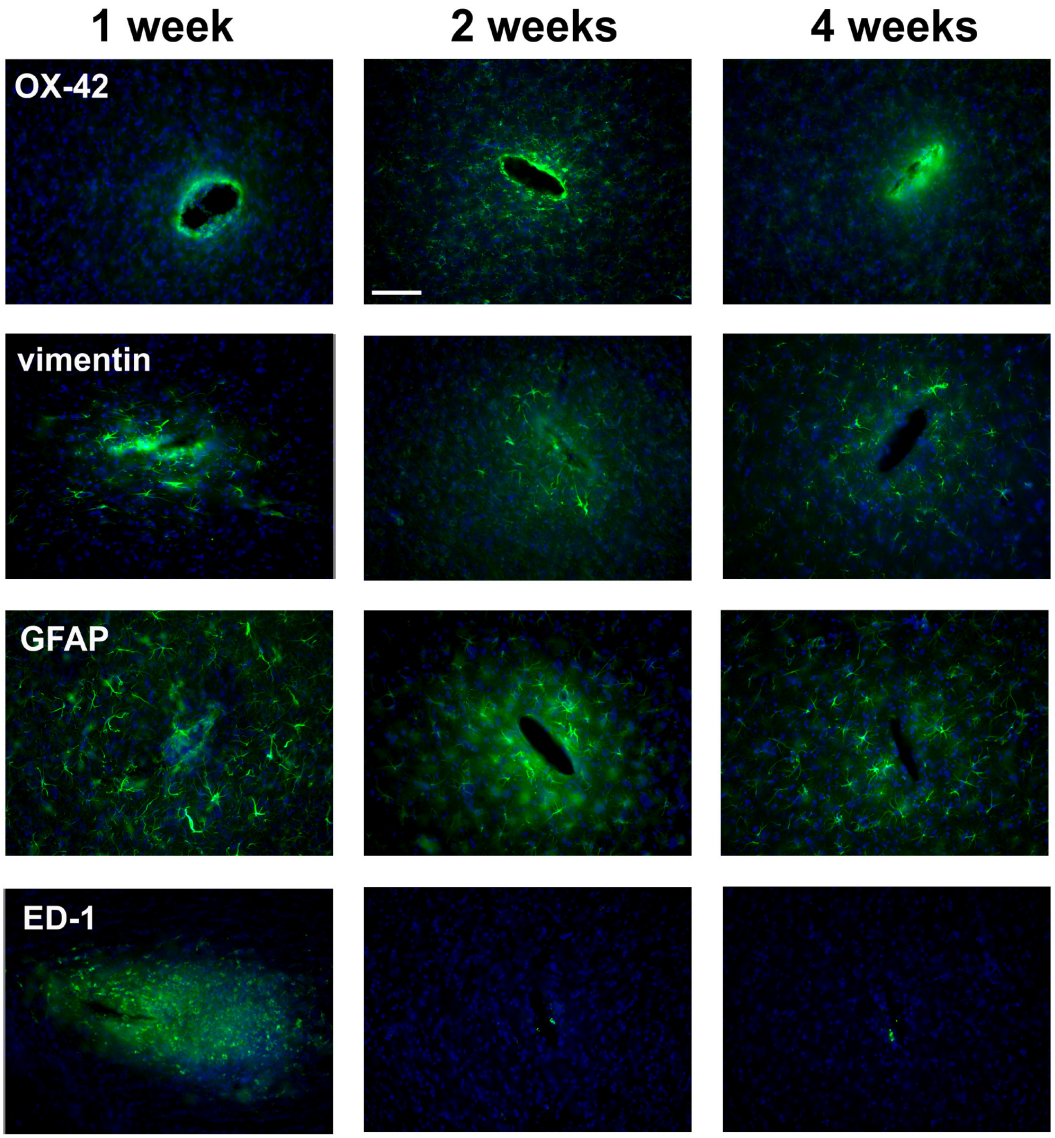

Figure U2-4. Temporal CNS host response to uncoated microelectrodes. Representative horizontal tissue sections stained for either OX-42, vimentin, GFAP, or ED-1 (all in green) at 1, 2, and 4 weeks are shown. Nuclei were counterstained in blue with the nuclear dye DAPI. Note the persistence of OX-42 immunoreactivity, the marked decline in ED-1, and the appearance of intensely $GFAP^{+}$ hypertrophied astrocytes. All sections were taken at the level of the cerebral cortex. Scale bar = 100 microns.

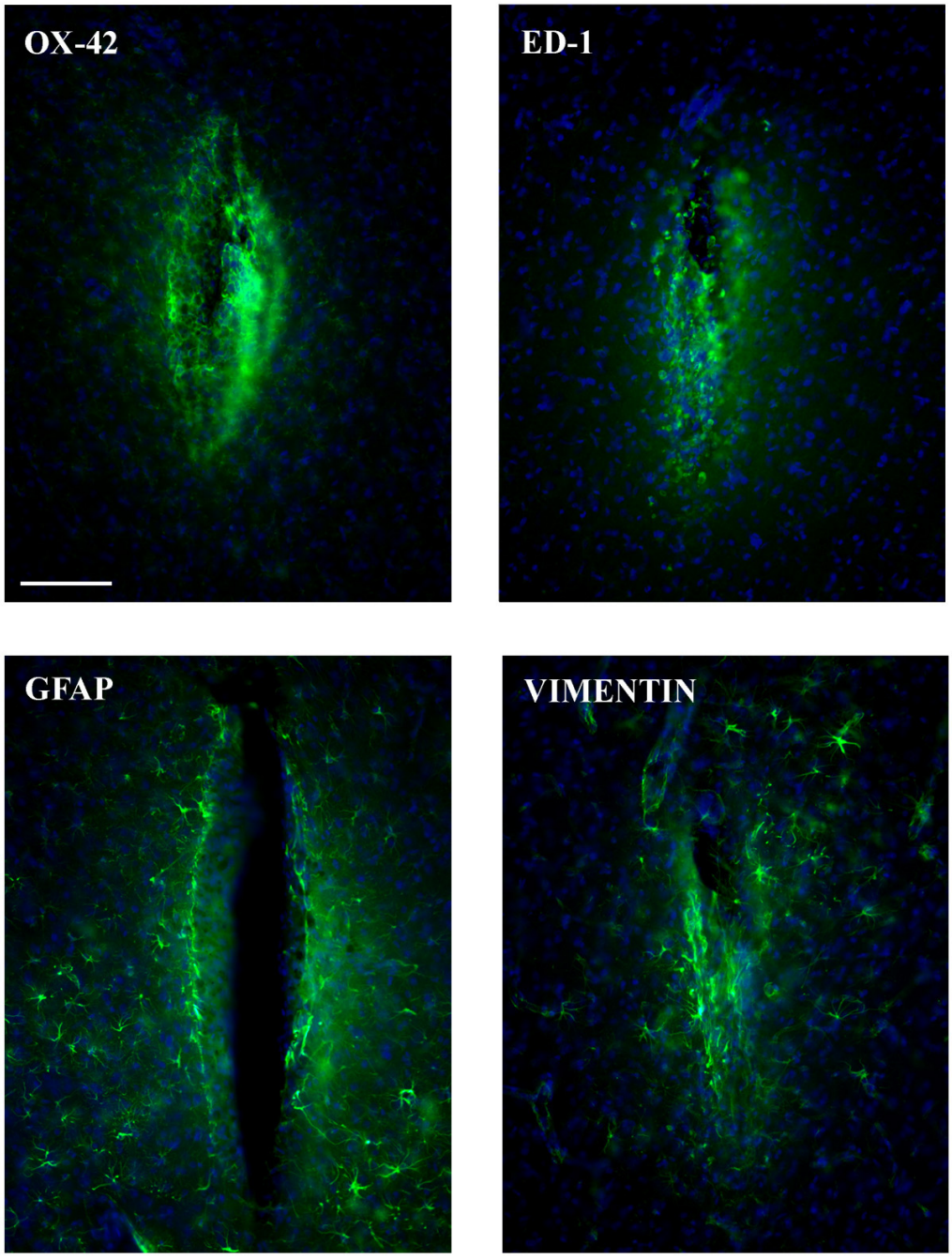

Figure U2-5. Representative coronal sections through the microelectrode tract at 2 weeks post-implantation. Note the dense layer of OX-42 immediately adjacent to the gap left by the retrieved microelectrode. A continuous wall of highly GFAP immunoreactive cells is evident along the electrode tract Nuclei were stained in blue with the nuclear dye DAPI. Scale bar = 100 microns.

The retrieved microelectrodes were also examined by immunostaining. Cellular material was evident on all the retrieved probes, however, the amount of attached cells varied between animals.

No clear correlation between the amount of attached cells and the duration of the implant was evident. However, microglia (or macrophages) were the only cell type found on the retrieved electrodes. They were found on both the electrode shaft as well on the recording sites. In a subset of retrieved microelectrodes, no detectable GFAP or beta-III-tubulin (for detecting neurons) was observed. Representative images of retrieved microelectrodes are shown in Figure U2-6.

CONCLUSIONS AND FUTURE WORK

Currently, we are examining selective cell attachment to a series of coated microelectrodes supplied by the University of Michigan. We intend to report on cell attachment and outgrowth on both fully-coated and site-only coated microelectrodes. Also to be included are competition type attachment assays, and a quantitative analysis of cell division (as assessed by BrdU labeling). Furthermore, we will conclude our analysis of the control untethered and uncoated electrodes by examining the tissue response at 12 weeks post implantation. We also intend to initiate another series of microelectrode implants, with specific emphasis on the host response to tethered probes and those with specific coatings.

REFERENCES

Biran, R., Noble, M., and P.A. Tresco (1999). Characterization of cortical astrocytes on materials of differing surface chemistry. J. Biomat. Mater. Res. 46: 150-159.

Manwaring, M., Biran, R., and P.A. Tresco (2001). Characterization of rat meningeal cultures on materials of differing surface chemistry. Biomaterials 22: 3155-3168.

Rogers, S., Letourneau, P., Palm, S., McCarthy, J., and L.T. Furcht (1983). Neurite extension by peripheral and central nervous system neurons in response to substratum-bound fibronectin and laminin. Dev. Biol. 98: 212-220.

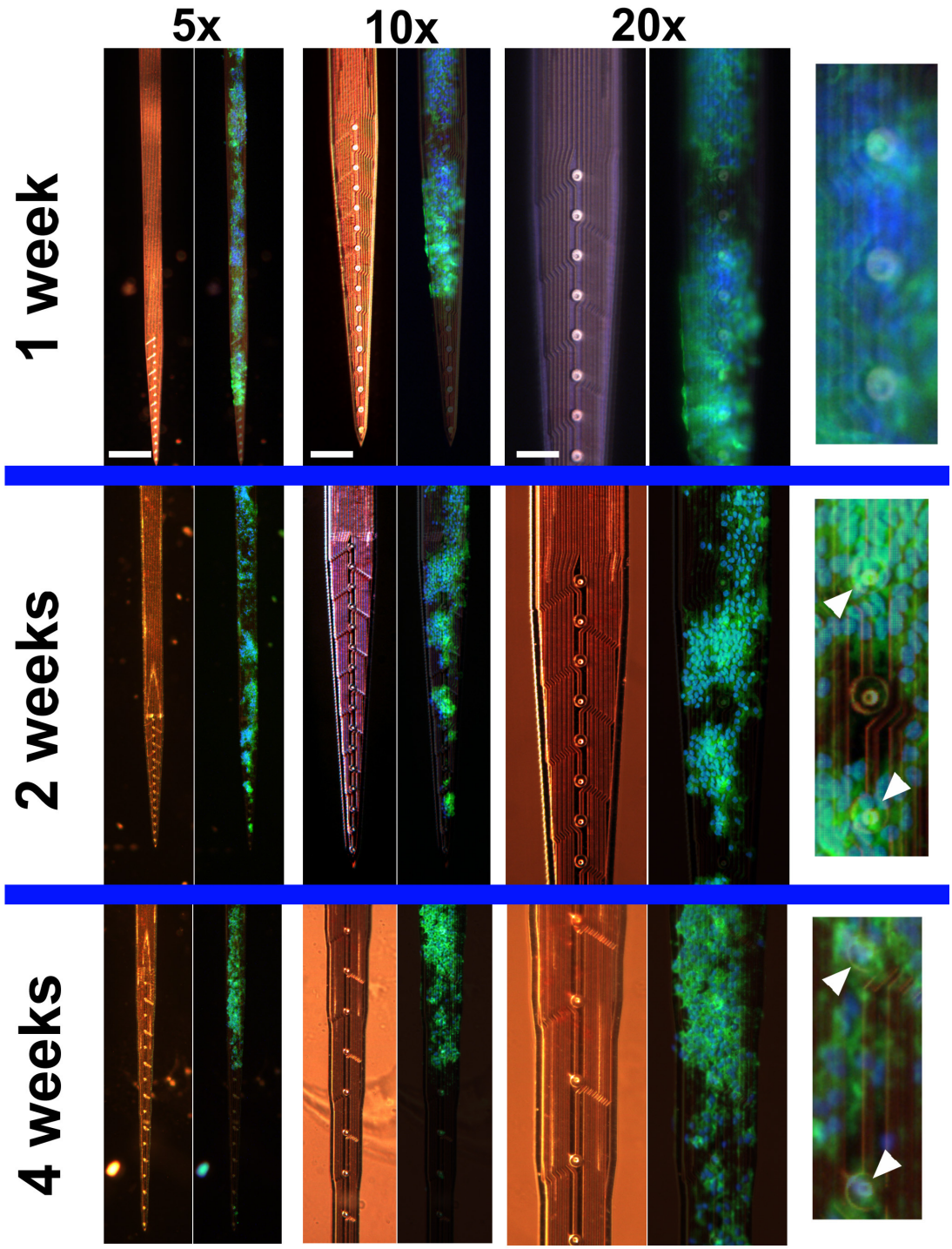

Figure U2-6. Most cells directly adherent to the retrieved microelectrodes are OX-42 (green) immunopositive. The rightmost panels are close-ups taken from the 20x images to their left. Arrowheads indicate recording sites in areas where it may be difficult to see them through the fluorescently-labeled cell layer. Nuclei were stained in blue with the nuclear dye DAPI. Scale bar in 5x column = 400 microns, in 10x column = 200 microns, in 20X column = 100 microns.